Universal spatiotemporal scaling of distortions in a drifting lattice

Pritha Dolai,[1] Abhik Basu,[2,*] and Aditi Simha[1,†]
[1]*Department of Physics, Indian Institute of Technology Madras, Chennai 600036, India*
[2]*Saha Institute of Nuclear Physics, 1/AF Bidhannagar, Calcutta 700064, India*
(Received 19 October 2016; revised manuscript received 17 January 2017; published 10 May 2017)

We study the dynamical response to small distortions of a lattice about its uniform state, drifting through a dissipative medium due to an external force, and show, analytically and numerically, that the fluctuations, both transverse and longitudinal to the direction of the drift, exhibit spatiotemporal scaling belonging to the Kardar-Parisi-Zhang universality class. Further, we predict that a colloidal crystal drifting in a constant electric field is linearly stable against distortions and the distortions propagate as underdamped waves.

DOI: 10.1103/PhysRevE.95.052115

I. INTRODUCTION

It is well known from elastic theory that distortions in a crystal at thermal equilibrium propagate as waves with a speed determined by the elastic constants of the lattice [1,2]. The response of a lattice drifting due to an external force through a dissipative medium was first addressed by Lahiri and Ramaswamy (LR) in Ref. [3]. The linear stability of the lattice was predicted to depend on certain model parameters that govern the strain dependence of the mobility of the lattice. The role of anharmonic effects and random fluctuations (possibly of nonequilibrium origin) on the macroscopic nature of steady states, including scaling properties, is still unknown. This potentially opens up the possibility that either the anharmonic effects drive the ensuing steady state away from its equilibrium counterpart, or leave the system macroscopically indistinguishable from a crystal in equilibrium. In this paper, we address these issues. Specifically, we ask: What is the macroscopic nature of the drifting nonequilibrium state?

The study of drifting lattices began with the work of Crowley [4] who predicted that an array of particles moving through a viscous fluid is unstable to clumping due to hydrodynamic forces alone, a result he verified experimentally by dropping steel balls into turpentine oil. The role of elastic and Brownian forces on this lattice instability was analyzed by Lahiri and Ramaswamy [3]. A set of continuum equations for the displacement fields of the drifting lattice, constructed using symmetry arguments, showed that the lattice was linearly unstable to clumping, even in the presence of elasticity. The role of nonlinearities and noise on the linear instability was not analyzed. Numerical studies of an equivalent lattice-gas model describing the coupled dynamics of concentration and tilt fields showed that the lattice was stable to distortions up to a critical Péclet number at which a nonequilibrium phase transition to a clumped state occurred.

In this work, we find that the nonequilibrium steady state of the drifting lattice is phenomenally different from its equilibrium counterpart. We show that small, long-wavelength lattice distortions exhibit spatiotemporal scaling both transverse and longitudinal to the direction of drift of the lattice and establish, analytically and numerically, that the fluctuations display dynamical scaling that belongs to the Kardar-Parisi-Zhang (KPZ) universality class [5]. As an example of this drifting nonequilibrium state, we analyze the dynamics of distortions in a colloidal crystal drifting in a constant electric field and show that it has a linearly stable state in which long wavelength distortions propagate as under damped waves. The wave speeds and the length scale beyond which these propagating waves can be detected are also calculated in terms of the driving force and the parameters defining their interactions.

II. DRIFTING LATTICES IN DISSIPATIVE MEDIA

For a driven, nonequilibrium system such as ours, the equations of motion for the degrees of freedom must be written down directly, by using symmetry arguments. Physically, the equations of motion for the displacement field $\mathbf{u}(\mathbf{r},t)$ of a lattice moving in a frictional medium, ignoring inertia completely, must obey the equation

$$\dot{\mathbf{u}} = \underline{\underline{\mathbf{M}}}(\nabla\mathbf{u}) \cdot \mathbf{F}_{\rm tot} = \underline{\underline{\mathbf{M}}}(\nabla\mathbf{u}) \cdot (\mathbf{F} + \underline{\underline{\mathbf{D}}}\nabla\nabla\mathbf{u} + \boldsymbol{\eta}). \quad (1)$$

Here, $\underline{\underline{\mathbf{M}}}$ is the mobility tensor that depends on the local lattice strain, $\mathbf{F}_{\rm tot}$ is the total force consisting of the external driving force $\mathbf{F}$, elastic forces due to lattice distortions $\underline{\underline{\mathbf{D}}}\nabla\nabla\mathbf{u}$ and the random force $\boldsymbol{\eta}$ acting on the particle due to the surrounding fluid. The mobility tensor has the form $\underline{\underline{\mathbf{M}}} = \underline{\underline{\mathbf{M_0}}} + \underline{\underline{\mathbf{A}}}(\nabla\mathbf{u}) + O(\nabla\mathbf{u})^2$ where $\underline{\underline{\mathbf{M_0}}}$ is the mean mobility of the undistorted lattice, $\underline{\underline{\mathbf{A}}}$ is the first-order correction to it due to lattice distortions and the successive terms higher-order corrections [3]. These terms arise from interactions between particles in the surrounding viscous medium.

For a lattice in the (x,y) plane drifting along the $\hat{z}$ direction the equations of motion for the displacement field $(\mathbf{u}_\perp, u_z)$ are isotropic in the transverse [$\perp$ or (x,y)] plane but not invariant under $z \to -z$. The equations hence have the form:

$$\dot{\mathbf{u}}_\perp = \lambda_1\partial_z\mathbf{u}_\perp + \lambda_2\nabla_\perp u_z + D_1\nabla_\perp^2\mathbf{u}_\perp + D_3\partial_z^2\mathbf{u}_\perp + O(\nabla u\nabla u) + \boldsymbol{\eta}_\perp, \quad (2)$$

$$\dot{u}_z = \lambda_3\nabla_\perp\cdot\mathbf{u}_\perp + \lambda_4\partial_z u_z + D_2\nabla_\perp^2 u_z + D_4\partial_z^2 u_z + D_5\partial_z\nabla_\perp\cdot\mathbf{u}_\perp + O(\nabla u\nabla u) + \eta_z. \quad (3)$$

These follow from Eq. (1) albeit in the frame of the drifting lattice. The constant term in (1) has hence been omitted. The λ_i s are phenomenological parameters arising from the

*abhik.basu@saha.ac.in; abhik.123@gmail.com
†phyadt@iitm.ac.in

strain dependence of the mobility and depend crucially on the details of the hydrodynamic interaction between particles in the system. They are proportional to the drift speed of the lattice. The D_i s are diffusion constants coming from elastic restoring forces in Eq. (1). $\eta_\perp$ and η_z are Gaussian white noise in the lattice plane and perpendicular to it, respectively. There are a total of nine quadratic nonlinearities, $O(\nabla u \nabla u)$ terms, in these equations which arise from the dependence of the λ_i s on the local concentration and tilt ($\nabla_\perp u_z$).

In this paper, we work with a simplified version of these equations in one dimension [3]. The displacement field $\mathbf{u}(\mathbf{r},t)$ of the lattice then has only two components (u_x,u_z) and only derivatives in x are considered; those along the direction of drift $\hat{z}$ are averaged out. With this simplification Eqs. (2), (3) reduce to

$$\dot{u}_x = \lambda_2 \partial_x u_z + \gamma_1 \partial_x u_x \partial_x u_z + D_1 \partial_x^2 u_x + \eta_x, \tag{4}$$

$$\dot{u}_z = \lambda_3 \partial_x u_x + \gamma_2 (\partial_x u_x)^2 + \gamma_3 (\partial_x u_z)^2 + D_2 \partial_x^2 u_z + \eta_z. \tag{5}$$

Only three quadratic nonlinearities are allowed by symmetry and only Eq. (5) has the KPZ nonlinearity $(\partial_x u_z)^2$. The equations are coupled at the linear level and can be decoupled, at the linear level, for fields that are appropriate linear combinations of u_x,u_z. The resulting equations are coupled KPZ equations [see Eqs. (12), (13)]. Coupled KPZ equations arise in various contexts such as the dynamic roughening of directed lines [6,7], stochastic lattice gases [8,9], magnetohydrodynamics [10–12], and anharmonic chains on a mesoscopic scale [13]. We refer the reader to Refs. [9,13–17] for a perspective on the subject and an extensive analysis of the equations. Its equivalence with the nonlinear fluctuating hydrodynamics for multicomponent driven stochastic lattice gases was established in Ref. [9]. This was tested using a Monte Carlo simulation of the two-component AHR (Arndt, Heinzel, and Rittenberg) model, which confirmed that the two modes satisfy KPZ scaling, including the scaling function and the dependence on the nonuniversal coefficients. Similar equations, arising in the context of anharmonic chains, have been dealt with using a one-loop approximation. Analytic predictions and numerical solutions of the corresponding mode-coupling equations establish KPZ scaling, including the nonuniversal scaling coefficient, for the propagative sound modes in the system [13]. Even the form of the scaling function for these modes was shown to be very close (differing by a few percent) to the KPZ scaling function.

Linearizing and Fourier transforming Eqs. (4), (5) in space and time, as in Ref. [3], yields the dispersion relations for the two modes of the system

$$\omega = \frac{-ik^2(D_1+D_2)}{2} \pm \frac{1}{2}\sqrt{4\lambda_2\lambda_3 k^2 - k^4 (D_1 - D_2)^2}, \tag{6}$$

where ω is the frequency and k the wave number of the mode. For long-wavelength (small-k) distortions this implies that the crystal is linearly stable only when $\lambda_2\lambda_3 > 0$. Symmetry arguments alone cannot *a priori* determine whether the lattice is stable as the signs of these parameters depend on the details of the interaction between particles, which is system dependent. For a sedimenting lattice the product $\lambda_2\lambda_3$ was calculated and found to be negative [3] implying a linear instability towards clumping. We calculate $\lambda_2\lambda_3$ for a colloidal crystal drifting due to an applied electric field before we address the effect of nonlinearities.

III. COLLOIDAL CRYSTAL IN AN ELECTRIC FIELD

Consider a one-dimensional (1D) lattice of colloidal particles of radius a with lattice spacing d in the x direction and the electric field $\mathbf{E}$ perpendicular to the lattice (as in Fig. 1). A single charged colloid drifts in the field with constant velocity, $\mathbf{V} = \xi \mathbf{E}$, where ξ is its mobility. Its motion results from a complex interplay of electrostatic, hydrodynamic, and thermal forces and its mobility depends on various parameters such as the thickness of the electric double layer of small counterions, surface properties, charge density, ion concentration, and lipophilicity of the colloid and the specific properties of counterions and salt ions. There is as yet no expression for the mobility applicable, in general, as a function of these parameters [18–21]. The mobility of a charged sphere, in the thin double layer limit, was first derived by Smoluchowski [22] to be $\xi_0 = \epsilon\zeta/\bar{\eta}$, where ϵ and $\bar{\eta}$ are the dielectric permittivity and viscosity of the colloidal solution and ζ the zeta potential on the surface of the sphere. For double layers of arbitrary thickness but small ζ, Smoluchowski's result for the mobility was modified by Henry to $\xi = \xi_0 f(\kappa a)$ where κ^{-1} is the Debye length [23] and $f(\kappa a)$ Henry's function, which is an increasing function of κa. The mobility of a particle is modified in the presence of other particles due to interactions between them. For two identical spherical particles of radius a, the mobility was derived using the method of reflections by Ennis *et al.* [24]. The electrophoretic velocity of a sphere in the presence of an identical sphere at a distance d is given by

$$\mathbf{V} = \frac{\xi}{4\pi}\{A_\parallel \mathbf{ee} + A_\perp(\mathbf{I}-\mathbf{ee}) + [B_\parallel \mathbf{ee} + B_\perp(\mathbf{I}-\mathbf{ee})]\} \cdot \mathbf{E}. \tag{7}$$

Here $\mathbf{e}$ is a unit vector along the line joining the two spheres and $\mathbf{I}$ the unit tensor of rank two. $A_{||}$, $A_\perp$, $B_{||}$, and $B_\perp$ have the form (keeping only the leading-order dependence on d): $A_{||} = 1 - (\frac{a}{d})^3$, $A_\perp = 1 + \frac{1}{2}(\frac{a}{d})^3$, $B_{||} = (\frac{a}{d})^3 \frac{L(\kappa a)}{f(\kappa a)}$, and $B_\perp = -(\frac{a}{d})^3 \frac{L(\kappa a)}{2f(\kappa a)}$. The function $L(\kappa a)$ decreases monotonically with κa. The dominant interaction between two particles, as implied by this result, decays as $1/d^3$. Both $f(\kappa a)$ and $L(\kappa a)$ tend to 1 as $\kappa a \to \infty$. In this limit the result for thin diffuse

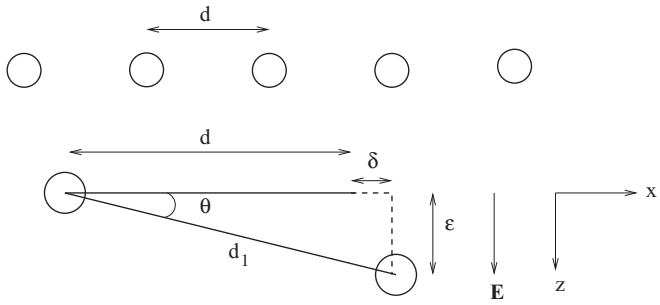

FIG. 1. Schematic diagram to show displacement fields. δ and ϵ are the displacements of a particle in x and z direction from its original position.

layers is recovered where particles do not interact with each other.

According to (7) a pair of particles at distance d apart (as in Fig. 1) move in the z direction with speed v_0 given by Eq. (7). If one of them is displaced by δ and ϵ along and perpendicular, respectively, to the lattice at some instant of time, the change in velocity Δv_x and Δv_z along the x and z directions due to the displacement are

$$\Delta v_x = C\left[\frac{3}{2}\left(\frac{\epsilon}{d}\right) - 6\left(\frac{\delta}{d}\right)\left(\frac{\epsilon}{d}\right)\right], \tag{8}$$

$$\Delta v_z = C\left[\frac{3}{2}\left(\frac{\delta}{d}\right) - 3\left(\frac{\delta}{d}\right)^2 + \frac{9}{4}\left(\frac{\epsilon}{d}\right)^2\right], \tag{9}$$

where $C \approx v_0(\frac{a}{d})^3(\frac{L(\kappa a)}{f(\kappa a)} - 1)$. Using the expressions for $L(\kappa a)$ and $f(\kappa a)$ from Ref. [24] we find that $L(\kappa a)/f(\kappa a) > 1$, for all κa and hence $C > 0$. This along with Eqs. (9), (8) implies that the spheres fall slower when they are closer and a displacement along the field travels in the $+x$ direction. The implications of this for the drifting lattice are evident. A perfect lattice drifts uniformly in the z direction. If the lattice were perturbed, say a region of it compressed, then it would drift slower in this region. With time, this results in a tilt of the interfacial region between the compressed and uncompressed regions. These tilted regions drift laterally as implied by Eq. (8). The direction of this lateral drift (given $C > 0$) is such that the tilted regions move apart dilating the compressed regions. The lattice is thus stable to distortions. If we approximate $\partial_x u_x \approx \frac{\delta}{d}$ and $\partial_x u_z \approx \frac{\epsilon}{d}$, then the expressions on the right-hand side (RHS) of Eqs. (8), (9) are exactly the terms on the RHS of Eqs. (4), (5). The coefficients λ_2, λ_3 for the drifting lattice can thus be obtained by summing the contributions of the nearest neighbors to the change in velocity Δv_x and Δv_z of a particle in the lattice. Our results for two particles allow us to conclude that $\lambda_2\lambda_3 > 0$ since C is always greater than zero. The speed of the propagating modes $v \propto \sqrt{\lambda_2\lambda_3} \approx C$. For particles of radius $a = 1\mu$m, $\kappa a = 2.5$, $d = 3a$ in an electric field of strength 150 V/m, we estimate the speed of the propagating modes to be 10 μm/s. These propagating modes dominate beyond a length scale $l_c \sim 2\pi D/\sqrt{\lambda_2\lambda_3}$. We estimate $l_c \approx 50\,d$ for this system. It should hence be possible to detect these modes in systems that are larger than l_c. A similar analysis for a 1D lattice drifting parallel to the electric field indicates that the lattice is linearly stable. This is a general result applicable to all drifting lattices. Having established that the lattice is linearly stable, we ask what is the effect of the nonlinearities and noise on this stable state.

IV. NONLINEARITIES AND FLUCTUATIONS

To analyze the effect of nonlinearities and fluctuations on the linearly stable state, approximate methods must be used as Eqs. (4)–(5) cannot be solved in closed form. Exact results pertaining to their spatial and temporal scaling behavior can be obtained using a dynamic renormalization group (DRG) analysis [25,26]. In particular, the roughness exponents χ_x, χ_z and dynamic exponents z_x, z_z of the fields u_x and u_z, respectively, defined by the scaling forms of their correlation functions

$$C^{xx}(x,t) = \langle u_x(x,t)u_x(0,0)\rangle = A_x|x|^{2\chi_x} f_x(x/t^{z_x}), \tag{10}$$

$$C^{zz}(x,t) = \langle u_z(x,t)u_z(0,0)\rangle = A_z|x|^{2\chi_z} f_z(x/t^{z_z}) \tag{11}$$

can be determined using this method. Here the functions f_x, f_z are dimensionless scaling functions of their arguments, and coefficients A_x, A_z are constants.

On scaling space as $x \to bx$, time as $t \to b^{z_i}t$ and the fields as $u_i(x,t) \to b^{\chi_i}u_i(bx, b^{z_i}t), i = x,z$, the correlation functions scale as $C^{xx}(x,t) \to b^{2\chi_x}C^{xx}(bx, b^{z_x}t)$, $C^{zz}(x,t) \to b^{2\chi_z}C^{zz}(bx, b^{z_z}t)$. If $z_x = z_z$, then the model displays strong dynamic scaling, otherwise weak dynamic scaling [8].

We begin by decoupling Eqs. (4), (5) at the linear level by defining the fields $\phi_\pm = u_x \pm \nu u_z$ where $\nu = \sqrt{\lambda_2/\lambda_3}$. In terms of $\phi_\pm$, they become

$$\dot{\phi}_+ - \frac{\alpha}{2}\partial_x\phi_+ + a_1(\partial_x\phi_+)^2 + b_1(\partial_x\phi_-)^2 + c_1(\partial_x\phi_+)(\partial_x\phi_-) = D_+\partial_x^2\phi_+ + \eta_+, \tag{12}$$

$$\dot{\phi}_- + \frac{\alpha}{2}\partial_x\phi_- + a_2(\partial_x\phi_+)^2 + b_2(\partial_x\phi_-)^2 + c_2(\partial_x\phi_+)(\partial_x\phi_-) = D_-\partial_x^2\phi_- + \eta_-. \tag{13}$$

The coefficient of the wave term $\frac{\alpha}{2} = \sqrt{\lambda_2\lambda_3}$, $\eta_\pm = \eta_x \pm \nu\eta_z$ and the coefficients of nonlinear terms depend on λ_2, λ_3, γ_1, γ_2, and γ_3. The zero-mean Gaussian white noises η_+, η_- are appropriate linear combinations of the noises η_x, η_z and have correlations $\langle\eta_+(x,t)\eta_+(x',t')\rangle = 2A_1\delta(x-x')\delta(t-t')$ and $\langle\eta_-(x,t)\eta_-(x',t')\rangle = 2A_2\delta(x-x')\delta(t-t')$. D_+ and D_- are the new diffusion constants. Noises η_+, η_- have nonzero cross correlations of the form $\langle\eta_+(x,t)\eta_-(x',t')\rangle = 2A_3\delta(x-x')\delta(t-t')$. Coupled equations of this type have been studied in considerable detail earlier [9,13–17]. Our approach here is to use dynamic renormalization group analysis to extract the scaling properties of these equations. For the special case with $\gamma_1 = 2\gamma_3$ and $\gamma_2/\gamma_3 = \lambda_3/\lambda_2$ Eqs. (12)–(13) reduce to two separate KPZ equations [3].

Fluctuations of ϕ_+ and ϕ_- propagate with a relative speed between them, thus one can eliminate the linear propagating term in either (12) or (13), but not simultaneously in both. At the linear level, the dynamics of ϕ_+ and ϕ_- are mutually decoupled. This implies $\chi_+ = 1/2 = \chi_-$ and $z_+ = 2 = z_-$, for the roughness and dynamic exponents defined by the correlation functions for ϕ_+ and ϕ_-, analogous to (10)–(11). This implies $\chi_x = 1/2 = \chi_z$ and $z_x = 2 = z_z$ in the linear theory.

With the nonlinear terms, Eqs. (12), (13) cannot be solved exactly and naive perturbative expansions in powers of the nonlinear coefficients yield diverging corrections in the long-wavelength limit. In order to deal with these long-wavelength divergences in a systematic manner, we employ perturbative one-loop Wilson momentum shell DRG [25,26]. This is implemented by first integrating out the dynamical fields $\phi_\pm(\mathbf{q},\omega)$ with wave vector $\Lambda/b < q < \Lambda$, $b > 1$, perturbatively up to the one-loop order using (12)–(13). Λ is the wave vector upper cutoff. We then rescale wave vectors by $q' = bq$, so that the upper cutoff is restored to Λ. The

frequency ω and the fields are also scaled appropriately [25,26]. The one-loop perturbation theory is constructed using the bare propagators and correlators of $\phi_\pm$. We work in the comoving frame of ϕ_+ where the bare propagators (in Fourier space) are of the form $G_0^+(k,\omega) = \frac{1}{D_+k^2+i\omega}$ and $G_0^-(k,\omega) = \frac{1}{D_-k^2+i(\omega-\alpha k)}$, for ϕ_+ and ϕ_-, respectively. Thus, at linear order $\phi_+(k,\omega) = G^+(k,\omega)\eta_+(k,\omega)$ and $\phi_-(k,\omega) = G^-(k,\omega)\eta_-(k,\omega)$ [see Fig. 4 for a diagrammatic representation of Eqs. (12), (13)]. In a similar manner, correlators of $\phi_\pm$ in the comoving frame of ϕ_+ are defined as $C_{\phi_+\phi_+}(k,\omega) = \frac{2A_1}{\omega^2+D_+^2k^4}$ and $C_{\phi_-\phi_-}(k,\omega) = \frac{2A_2}{(\omega-\alpha k)^2+D_-^2k^4}$. Notice that since each of (12), (13) can be reduced to the standard KPZ equation [5] upon setting appropriate coupling constants to zero, the lowest-order perturbative corrections to $D_\pm, A_1, A_2, a_1$, and a_2 can clearly be classified into two categories: (i) KPZ type, which survive in the KPZ limit, and (ii) non-KPZ type, which vanish in that limit. The KPZ-type diagrams are formally identical to those in the pure KPZ problem [5]. The relevant one-loop Feynman diagrams are shown in Fig. 5 and listed in the Appendix. Retaining only the dominant contributions (all of which arise from the respective KPZ-type diagrams), we find the corrections to be

$$\tilde{A}_1 = A_1\left[1 + \frac{a_1^2 A_1}{\pi D_+^3}\int_{\Lambda/b}^{\Lambda}\frac{1}{q^2}dq\right], \tag{14}$$

$$\tilde{A}_2 = A_2\left[1 + \frac{A_1^2 a_2^2}{\pi A_2 D_+^3}\int_{\Lambda/b}^{\Lambda}\frac{1}{q^2}dq\right], \tag{15}$$

$$\tilde{D}_+ = D_+\left[1 + \frac{A_1 a_1^2}{\pi D_+^3}\int_{\Lambda/b}^{\Lambda}\frac{k^2}{q^2}dq\right], \tag{16}$$

$$\tilde{D}_- = D_-\left[1 + \frac{A_1 a_2 c_1}{\pi 2 D_+^2 D_-}\int_{\Lambda/b}^{\Lambda}\frac{k^2}{q^2}dq\right]. \tag{17}$$

None of the vertices a_1, b_1, c_1, a_2, b_2, and c_2 receive any fluctuation corrections at the one-loop order [27]. Under scalings $x \to bx$, $t \to b^z t$, $\phi_+ \to b^{\chi_+}\phi_+$, and $\phi_- \to b^{\chi_-}\phi_-$, the parameters scale as $A_1 \to b^{z-1-2\chi_+}A_1$, $A_2 \to b^{z-1-2\chi_-}A_2$, $D_\pm \to b^{z-2}D_\pm$. On rescaling the momentum cutoff and taking the limit $\delta l \to 0$, we get the recursion relations

$$\begin{aligned}
\frac{dD_+}{dl} &= D_+[z-2+g],\\
\frac{dA_1}{dl} &= A_1[z-1-2\chi_+ + g],\\
\frac{dD_-}{dl} &= D_-\left[z-2+\frac{1}{2}mnrg\right],\\
\frac{dA_2}{dl} &= A_2[z-1-2\chi_- + pn^2 g],
\end{aligned} \tag{18}$$

where the coupling constant $g \equiv \frac{A_1 a_1^2}{\pi D_+^3}$ and dimensionless constants $m = \frac{D_+}{D_-}$, $p = \frac{A_1}{A_2}$, $n = \frac{a_2}{a_1}$, and $r = \frac{c_1}{a_1}$. The renormalized coupling g then obeys

$$\frac{dg}{dl} = g[-2g+1], \tag{19}$$

giving the stable RG fixed point $g^* = 1/2$. The scaling exponents can be extracted from the equations $\frac{dD_+}{dl} = \frac{dA_1}{dl} = \frac{dD_-}{dl} = \frac{dA_2}{dl} = 0$ at the RG fixed point. This gives $z = 3/2$ and $\chi_+ = \chi_- = 1/2$, which belong to the KPZ universality class. Strong dynamic scaling prevails as the dynamic exponents for both the fields ϕ_+ and ϕ_- are the same. Since u_x and u_z can be written as linear combinations of ϕ_+ and ϕ_-, we have $\chi_x = \chi_z = 1/2$ and $z_x = z_z = 3/2$. The presence of propagating modes here is crucial; they render the so-called non-KPZ nonlinearities irrelevant in the long-wavelength limit so the model displays KPZ universality.

Having obtained the scaling exponents in the comoving frame of ϕ_+, we now argue that the values of these exponents are the same in all reference frames connected by the Galilean transformation [27]. Consider the correlation function, $C_+(x_1-x_2,t_1-t_2) = \langle\phi_+(x_1,t_1)\phi_+(x_2,t_2)\rangle$: under a Galilean transformation, $t_{1,2} \to t_{1,2}$, $x_{1,2} \to x_{1,2} + \mathsf{v}t$, where t is the time and v the Galilean boost. $x_1 - x_2$ and $t_1 - t_2$ are unchanged, hence so is C_+. The scaling exponents are thus the same in all frames connected by Galilean transformations.

The scaling behavior of the displacement fields u_x and u_z can also be obtained numerically by integrating Eqs. (4), (5). The correlation functions $C^{xx}(x,t)$ and $C^{zz}(x,t)$ can be calculated from the solutions of these equations. The equations of motion for u_x and u_z are simulated with diffusion constants $D_1 = D_2 = 1$, phenomenological parameters $\lambda_2 = 0.1$, $\lambda_3 = 0.2$, coefficients of nonlinear terms $\gamma_1 = 1.0$, $\gamma_2 = 2.0$, and $\gamma_3 = 10.0$ and time step $dt = 0.01$. We simulate a system of 2×10^4 particles with random initial conditions. The initial conditions are specified entirely by the displacement field $\mathbf{u}(\mathbf{r},t)$ at each lattice site. The displacements u_x and u_z at each site are chosen from a uniform distribution of random numbers between 0 and 1. We impose periodic boundary conditions. The noise in the equations are Gaussian random variables with zero mean and variances $2N_1dt, 2N_2dt$ respectively. Log-log plots of $C^{xx}(x,0)$ and $C^{zz}(x,0)$ are shown in Fig. 2 (top). The data are averaged over several realizations of the noise. We obtain $\chi_x = 0.47 \pm 0.06$, $\chi_z = 0.485 \pm 0.015$. Similarly, the log-log plots of $C^{xx}(0,t)$ and $C^{zz}(0,t)$ shown in Fig. 2 (bottom) yield $z_x = 1.45 \pm 0.05$, $z_z = 1.49 \pm 0.06$, which are the same as the dynamic exponent for the KPZ universality class, within error bars. Our numerical results are thus in close agreement with the DRG results. Figure 3 shows the correlation functions for different system sizes L collapse on each other on scaling t by L^z and correlations by L^{χ_i}, for $i = x,z$. This clearly establishes universal scaling in the model. Technical details of our numerical studies can be found in the Appendix.

V. CONCLUSIONS AND OUTLOOK

We have shown that a colloidal crystal drifting in an electric field is linearly stable, with long-wavelength lattice distortions propagating as waves. For particles of radius $a = 1\mu$m, $\kappa a = 2.5$, $d = 3a$ in an electric field of strength 150 V/m, we estimate the speed of the propagating modes to be 10 μm/s. Using renormalization group methods we

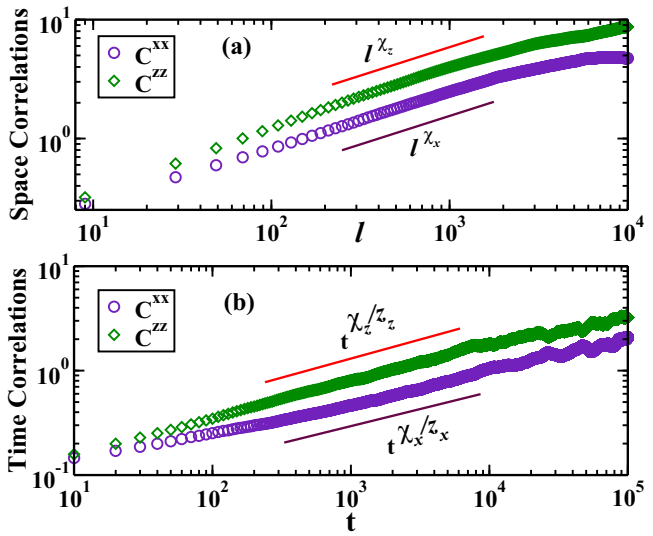

FIG. 2. (a) (top) Log-log plot of equal-time correlators $C^{xx}(l,t=0)$ and $C^{zz}(l,t=0)$ versus spatial separation l and (b) (bottom) log-log plots of equal space-point time-dependent correlators $C^{xx}(l=0,t)$ and $C^{zz}(l=0,t)$ versus t. Slopes yield exponents χ_x,χ_z and $\chi_x/z_x,\chi_z/z_z$, respectively (see text).

establish that, in the drifting steady state, lattice distortions both transverse and longitudinal to the lattice, display strong dynamic scaling with dynamic exponent 3/2 and belongs to the KPZ universality class. A numerical analysis of the equations for the displacement fields confirm these results.

The notion of universality survives even for driven elastic media. However, unlike equilibrium, this universal behavior is controlled by the drive, displaying 1D KPZ scaling. While extending our analysis to higher dimensions may be nontrivial, we can comment that in higher ($D>1$) dimensions there should be one longitudinal and $D-1$ transverse modes. The presence of propagating waves should make the system anisotropic. Thus, it is unlikely that the fluctuations in higher dimensions belong to the KPZ universality class. We look forward to theoretical attempts in understanding the universal properties of the fluctuations at higher D and experimental tests of our predictions for propagating modes in drifting colloidal crystals.

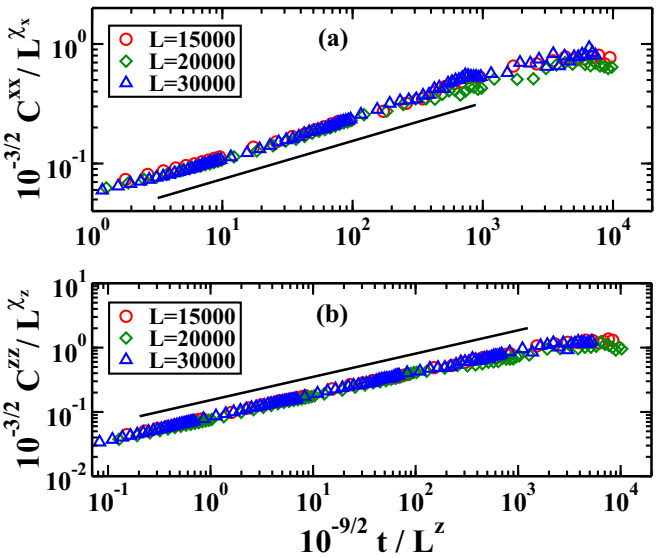

FIG. 3. Log-log plots of (top) C^{xx} and (bottom) C^{zz} as functions of t/L^z, showing data collapse on to single curves after scaling.

ACKNOWLEDGMENTS

We thank S. Ramaswamy for introducing the problem to us and his insights into it. A.B. wishes to thank the Alexander von Humbolt Stiftung (Germany) for partial financial support under the Research Group Linkage Programme scheme (2016).

APPENDIX A: EQUATIONS OF MOTION AND DIAGRAMMATIC EXPANSIONS

The equations of motion for $\phi_\pm$ are

$$\dot{\phi}_+ - \frac{\alpha}{2}\partial_x\phi_+ + a_1(\partial_x\phi_+)^2 + b_1(\partial_x\phi_-)^2 + c_1(\partial_x\phi_+)(\partial_x\phi_-) = D_+\partial_x^2\phi_+ + \eta_+ \quad \text{(A1)}$$

$$\dot{\phi}_- + \frac{\alpha}{2}\partial_x\phi_- + a_2(\partial_x\phi_+)^2 + b_2(\partial_x\phi_-)^2 + c_2(\partial_x\phi_+)(\partial_x\phi_-) = D_-\partial_x^2\phi_- + \eta_-, \quad \text{(A2)}$$

where the coefficient of wave term $\frac{\alpha}{2} = \sqrt{\lambda_2\lambda_3}$, noises are $\eta_\pm = f_x \pm \sqrt{\frac{\lambda_2}{\lambda_3}} f_z$ and other coefficients are $a_1 = -\frac{(\gamma_1+\gamma_3)}{4}\sqrt{\frac{\lambda_3}{\lambda_2}} - \frac{\gamma_2}{4}\sqrt{\frac{\lambda_2}{\lambda_3}}$, $b_1 = -\frac{(\gamma_3-\gamma_1)}{4}\sqrt{\frac{\lambda_3}{\lambda_2}} - \frac{\gamma_2}{4}\sqrt{\frac{\lambda_2}{\lambda_3}}$, $c_1 = \frac{\gamma_3}{2}\sqrt{\frac{\lambda_3}{\lambda_2}} - \frac{\gamma_2}{2}\sqrt{\frac{\lambda_2}{\lambda_3}}$, and $a_2 = -b_1$, $b_2 = -a_1$, and $c_2 = -c_1$. In the special case with $\gamma_1 = 2\gamma_3$ and $\gamma_2/\gamma_3 = \lambda_3/\lambda_2$ Eqs. (A1)–(A2) reduce to two separate KPZ equations [5].

$G_0^+(k,\omega)$ and $G_0^-(k,\omega)$ are the bare propagators for ϕ_+ and ϕ_-, respectively, in the comoving frame of ϕ_+ and have the form

$$G_0^+(k,\omega) = \frac{1}{D_+k^2 + i\omega}, \qquad G_0^-(k,\omega) = \frac{1}{D_-k^2 + i(\omega-\alpha k)}. \quad \text{(A3)}$$

The correlators of $\phi_\pm$ in the Fourier space are defined in the comoving frame of ϕ_+ as

$$C_{\phi_+\phi_+}(k,\omega) = \frac{2A_1}{\omega^2 + D_+^2k^4},$$
$$C_{\phi_-\phi_-}(k,\omega) = \frac{2A_2}{(\omega-\alpha k)^2 + D_-^2k^4}. \quad \text{(A4)}$$

Our perturbative dynamic renormalization group (DRG) calculation may be represented diagrammatically [25]. The symbols, that we use are explained in Fig. 4.

APPENDIX B: PROPAGATOR RENORMALIZATION

There are four one-loop diagrams, which contribute to the propagator renormalization of $\phi_\pm$. Figure 5 shows the relevant diagrams for propagator renormalization for ϕ_+.

The renormalized propagator $G^+(k,\omega)$ can be written as

$$G^+(k,\omega) = G_0^+(k,\omega) + T_1 + T_2 + T_3 + T_4, \quad \text{(B1)}$$

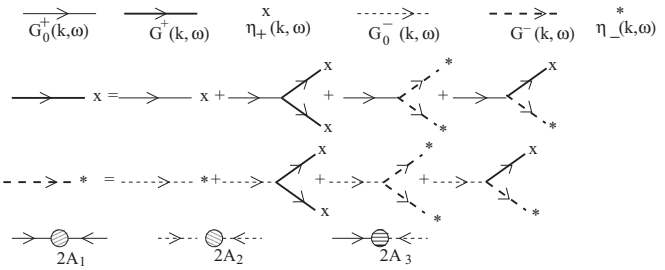

FIG. 4. Diagrammatic representation of the propagators and noise for ϕ_+ and ϕ_-. Perturbation expansion for the propagators $G_+(k,\omega)$, $G_-(k,\omega)$. Contracted noise A_1, A_2, A_3.

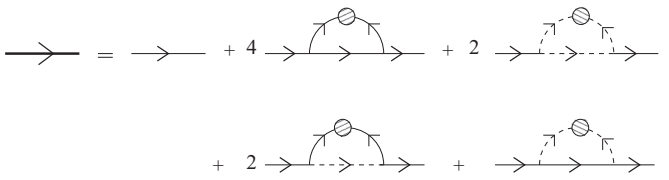

FIG. 5. One-loop diagrams for propagator renormalization.

where T_1 and T_2 contain contributions only from ϕ_+ and ϕ_-, respectively, and T_3, T_4 are the contributions from both the fields. We calculate the individual contributions below.

$$T_1 = \frac{8A_1a_1^2G_0^+(k,\omega)^2}{(2\pi)^2}\int dq\int_{-\infty}^{\infty} d\Omega[q(k-q)][-qk]G_0^+(q,\Omega)G_0^+(-q,-\Omega)G_0^+(k-q,\omega-\Omega)$$
$$= \frac{8A_1a_1^2G_0^+(k,\omega)^2}{(2\pi)^2}\int dq\int_{-\infty}^{\infty} d\Omega\frac{[q(k-q)][-qk]}{[D_+q^2+i\Omega][D_+q^2-i\Omega][D_+(k-q)^2-i\Omega]}. \tag{B2}$$

After angular integration T_1 behaves as $\sim\int dq\,\frac{\pi k(k-q)}{D_+^2[k^2-2kq+2q^2]} \approx k^2\int\frac{dq}{k^2-2kq+2q^2} \sim k^2 I_a$ where $I_a \sim \frac{1}{k}$. This is the contribution that survives in the KPZ limit of the model equations. Next we calculate the contribution coming from the second diagram, which scales as

$$T_2 \approx \int dq\int_{-\infty}^{\infty} d\Omega[q(k-q)][-qk]G_0^-(q,\Omega)G_0^-(-q,-\Omega)G_0^-(k-q,\omega-\Omega)$$
$$\approx \int dq\int_{-\infty}^{\infty}\frac{d\Omega[q(k-q)][-qk]}{[D_-q^2+i\Omega-i\alpha q][D_-q^2-i\Omega+i\alpha q][D_-(k-q)^2-i\Omega-i\alpha(k-q)]}$$
$$\approx \int dq\frac{\pi k(k-q)}{D_-[i\alpha k - D_-(k^2-2kq+2q^2)]} \approx k^2 I_b, \tag{B3}$$

where $I_b \sim \frac{1}{\sqrt{k}}$. Thus, T_1 is more divergent compared to T_2. The third diagram has a contribution

$$T_3 \approx \int dq\int_{-\infty}^{\infty} d\Omega\frac{[q(k-q)][-qk]}{[D_+q^2+i\Omega][D_+q^2-i\Omega][D_-(k-q)^2-i\Omega-i\alpha(k-q)]}$$
$$\approx \int\frac{dq}{D_-q^2-D_-(k-q)^2+i\alpha(k-q)} \sim k^2 I_c, \tag{B4}$$

where $I_c \sim -\ln k$ and the contribution from the last diagram is $T_4 \sim -k^2\int\frac{dq}{[i\alpha q - D_-q^2 - D_+(k-q)^2]} = k^2 I_d$ with $I_d \sim -\ln k^2$. So, T_1 is the most relevant diagram, which gives the renormalized propagator for ϕ_+ of the form

$$G^+ = G_0^+ - \frac{A_1a_1^2G_0^+(k,\omega)^2}{D_+^2\pi}\int_{\Lambda/b}^{\Lambda}\frac{k^2}{q^2}dq. \tag{B5}$$

Similarly, we find the renormalized propagator for ϕ_- and will be of the form

$$G^- = G_0^- - \frac{A_1a_2c_1G_0^-(k,\omega)^2}{2D_+^2\pi}\int_{\Lambda/b}^{\Lambda}\frac{k^2}{q^2}dq. \tag{B6}$$

Notice that in the hydrodynamic limit $k\to 0$, the dominant corrections to both G_0^+ and G_0^- are from the contributions that survive in the KPZ limit of the model. From the corrections to G_0^+ and G_0^-, we obtain the fluctuation corrected diffusion constants:

$$\tilde{D}_+ = D_+\left[1+\frac{A_1a_1^2}{\pi D_+^3}\int_{\Lambda/b}^{\Lambda}\frac{k^2}{q^2}dq\right]$$
$$\tilde{D}_- = D_-\left[1+\frac{A_1a_2c_1}{2\pi D_+^2D_-}\int_{\Lambda/b}^{\Lambda}\frac{k^2}{q^2}dq\right]. \tag{B7}$$

APPENDIX C: NOISE RENORMALIZATION

Consider now the noise renormalization for ϕ_+ field. The corresponding one-loop corrections receive contributions from one diagram that survives in the KPZ limit and one that

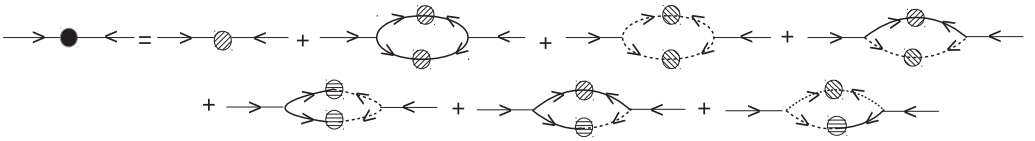

FIG. 6. One-loop diagrams for the renormalization of A_1.

vanishes in the KPZ limit. The diagrammatic representation of the perturbation series for the noise renormalization of A_1 is shown in Fig. 6.

The first one is given by

$$I_1 \sim \int_{\Lambda/b}^{\Lambda} dq \int_{-\infty}^{\infty} d\Omega \frac{q^2(k-q)^2}{[\Omega^2 + D_+^2 q^4][\Omega^2 + D_+^2 (k-q)^4]} \sim \int_{\Lambda/b}^{\Lambda} dq \frac{1}{k^2 + 2q^2 - 2kq} \sim \int_{\Lambda/b}^{\Lambda} \frac{dq}{q^2 + k^2/2}, \tag{C1}$$

which survives in the KPZ limit of the model. The additional contribution that vanishes in that limit is

$$I_2 \sim \int_{\Lambda/b}^{\Lambda} dq \int_{-\infty}^{\infty} \times d\Omega \frac{q^2(k-q)^2}{[(\Omega - \alpha q)^2 + D_-^2 q^4][(\Omega + \alpha(k-q))^2 + D_-^2 (k-q)^4]} \sim \int_{\Lambda/b}^{\Lambda} dq \frac{k^2 - 2kq + 2q^2}{D_- k^2 \alpha^2 + (k^2 - 2kq + 2q^2)^2 D_-^3}. \tag{C2}$$

The first contribution, I_1 is the dominant contribution in the thermodynamic limit $k^2 \to 0$ and I_2 is subleading. This may be understood as follows. Notice that the most significant (or the dominant) contribution to both I_1 and I_2 from the lower (i.e., small-q) limits of the integrals, which are controlled by k^2. Set $q = 0$ in both the integrands in I_1 and I_2: The respective integrands scale as $\sim \frac{1}{k^2}$ and $\sim \frac{k^2}{k^2 + k^4}$. For small enough k^2, $k^2 \gg k^4$, yielding $I_1 \gg I_2$ in the limit $k \to 0$, establishing the dominance of I_1 over I_2 in the limit $k \to 0$.

There are four more diagrams (see Fig. 6) for noise correlations whose contributions are clearly subdominant to the contribution from I_1 above. Thus, in the long-wavelength limit, I_1, the contribution that is nonvanishing in the KPZ limit of the model, determines the fluctuation correction to A_1. We then have

$$\tilde{A}_1 = A_1 + \frac{a_1^2 A_1^2}{\pi D_+^3} \int_{\Lambda/b}^{\Lambda} \frac{1}{q^2} dq. \tag{C3}$$

Similarly, renormalized A_2 will be

$$\tilde{A}_2 = A_2 + \frac{A_1^2 a_2^2}{\pi D_+^3} \int_{\Lambda/b}^{\Lambda} \frac{1}{q^2} dq. \tag{C4}$$

Again, the dominant contribution in the hydrodynamic limit is the contribution that survives in the KPZ limit of the model.

APPENDIX D: VERTEX RENORMALIZATION

The diagrams that contribute to the vertex renormalization for a_1 are shown in Fig. 7. Renormalized vertex $\tilde{a}_1 = a_1(1 + \Gamma_1 + \Gamma_2 + \Gamma_3)$ where Γ_1, Γ_2, and Γ_3 are three different vertices as shown in the figure where $\Gamma_1 = \frac{2a_1^2 A_1}{\pi D_+^3} \int_{\Lambda/b}^{\Lambda} \frac{dq}{q^2}$ and $\Gamma_2 = \Gamma_3 = -\frac{a_1^2 A_1}{\pi D_+^3} \int_{\Lambda/b}^{\Lambda} \frac{dq}{q^2}$. So $\tilde{a}_1 = a_1$. There are similar relevant diagrams for b_1 renormalization, which also give $\tilde{b}_1 = b_1$. Similarly, it can be shown that all the vertices a_1, b_1, c_1, a_2, b_2, and c_2 receive no fluctuation corrections that diverge in the limit $k \to 0$. We discard all the finite corrections in the spirit of DRG calculations.

APPENDIX E: FLOW EQUATIONS

Of the total momentum range $0 < |q| < \Lambda$, the high-momenta components $\Lambda e^{-\delta l} < |q| < \Lambda$ are integrated out and we rescale in such a way so that the momentum cutoff remains the same. Taking the limit $\delta l \to 0$, we get the recursion relations

$$\begin{aligned} \frac{dD_+}{dl} &= D_+[z - 2 + g] \\ \frac{dA_1}{dl} &= A_1[z - 1 - 2\chi_+ + g] \\ \frac{dD_-}{dl} &= D_-\left[z - 2 + \frac{1}{2} mnrg\right] \\ \frac{dA_2}{dl} &= A_2[z - 1 - 2\chi_- + pn^2 g], \end{aligned} \tag{E1}$$

where the coupling constant $g \equiv \frac{A_1 a_1^2}{\pi D_+^3}$ and some dimensionless constants are $m = \frac{D_+}{D_-}$, $p = \frac{A_1}{A_2}$, $n = \frac{a_2}{a_1}$, and $r = \frac{c_1}{a_1}$. The coupling constant has a flow equation $\frac{dg}{dl} = g[-2g + 1]$, which gives the stable RG fixed point $g^* = 1/2$. Those dimensionless constants m, p, n, and r have the flow equations $\frac{dm}{dl} = m[1 - \frac{1}{2} nrm]g$, $\frac{dp}{dl} = p[2(\chi_- - \chi_+) + (1 - np^2)g]$, $\frac{dn}{dl} = n(\chi_+ - \chi_-)$, and $\frac{dr}{dl} = r(\chi_- - \chi_+)$. Under the scale transformations $x \to bx$, $t \to b^z t$, $\phi_+ \to b^{\chi_+} \phi_+$, and $\phi_- \to b^{\chi_-} \phi_-$. To get the fixed points we should set the left-hand side of the flow equations equal to zero. Flow equations of m, p, n, and r give $n^* r^* m^* = 2$, $p^{*2} n^* = 1$, and $\chi_+ = \chi_-$. We use these relations and put $\frac{dD_+}{dl} = \frac{dA_1}{dl} = \frac{dD_-}{dl} = \frac{dA_2}{dl} = 0$, which give the exponents $z = 3/2$ and $\chi_+ = \chi_- = 1/2$, which belong to the KPZ universality class.

APPENDIX F: NUMERICAL SIMULATION

We numerically integrate Eqs. (2)– (3) in the main text, calculate the time-dependent correlation functions of u_x and u_z, which yield the scaling exponents in the hydrodynamic

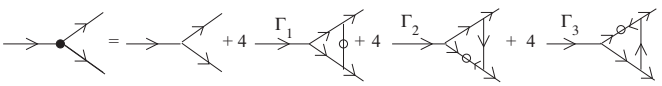

FIG. 7. One-loop diagrams that contribute to the fluctuation-corrections to the vertex a_1.

limit, and compare with the DRG results. The discretized equations used for numerical simulation are as follows:

$$\begin{aligned} u_x(x,t+\Delta t) = u_x(x,t) &+ \frac{\lambda_2}{2}[u_z(x+1,t) - u_z(x-1,t)]dt \\ &+ \frac{\gamma_1}{4}[u_x(x+1,t) - u_x(x-1,t)] \\ &\times [u_z(x+1,t) - u_z(x-1,t)]dt \\ &+ D_1[u_x(x+1,t) - 2u_x(x,t) \\ &+ u_x(x-1,t)]dt + \sqrt{2N_1 dt}\,\zeta_1(x,t) \end{aligned} \tag{F1}$$

$$\begin{aligned} u_z(x,t+\Delta t) = u_z(x,t) &+ \frac{\lambda_3}{2}[u_x(x+1,t) - u_x(x-1,t)]dt \\ &+ \frac{\gamma_2}{4}[u_x(x+1,t) - u_x(x-1,t)]^2 dt \\ &+ \frac{\gamma_3}{4}[u_z(x+1,t) - u_z(x-1,t)]^2 dt \\ &+ D_2[u_z(x+1,t) - 2u_z(x,t) + u_z(x-1,t)]dt \\ &+ \sqrt{2N_2 dt}\,\zeta_2(x,t). \end{aligned} \tag{F2}$$

ζ_1 and ζ_2 are Gaussian random variables with zero mean and variances $2N_1dt, 2N_2dt$, respectively. In the simulation, random initial conditions were used with periodic boundary conditions.

Roughness exponents are defined by the spatial scaling of the equal-time correlators $C^{xx}(l,0) \sim l^{\chi_x}$ and $C^{zz}(l,0) \sim l^{\chi_z}$ where $l = |x' - x|$. The growth exponent is defined through the correlation function with a time delay $C^{xx}(0,t) \sim t^{\beta_x}$ and $C^{zz}(0,t) \sim t^{\beta_z}$. These two exponents define dynamic exponents: $z_x = \chi_x/\beta_x$ and $z_z = \chi_z/\beta_z$. These correlation functions are shown in Fig. 2 of the main text. The exponents derived from fits to the data are mentioned in the main text.

[1] L. D. Landau and E. M. Lifshitz, *Theory of Elasticity* (Pergamon Press, Oxford, 1965).
[2] P. C. Martin, O. Parodi, and P. S. Pershan, Phys. Rev. A **6**, 2401 (1972).
[3] R. Lahiri and S. Ramaswamy, Phys. Rev. Lett. **79**, 1150 (1997).
[4] J. M. Crowley, J. Fluid. Mech. **45**, 151 (1971).
[5] M. Kardar, G. Parisi, and Y.-C. Zhang, Phys. Rev. Lett. **56**, 889 (1986).
[6] D. Ertas and M. Kardar, Phys. Rev. Lett. **69**, 929 (1992).
[7] D. Ertas and M. Kardar, Phys. Rev. E **48**, 1228 (1993).
[8] D. Das, A. Basu, M. Barma, and S. Ramaswamy, Phys. Rev. E **64**, 021402 (2001).
[9] P. L. Ferrari, T. Sasamoto, and H. Spohn, J. Stat. Phys. **153**, 377 (2013).
[10] A. Basu, J. K. Bhattacharjee, and S. Ramaswamy, Euro. Phys. J. B **9**, 725 (1999).
[11] J. Fleischer and P. H. Diamond, Phys. Rev. E **58**, R2709(R) (1998).
[12] S. Yanase, Phys. Plasmas **4**, 1010 (1997).
[13] H. Spohn, J. Stat. Phys. **154**, 1191 (2014).
[14] C. B. Mendl and H. Spohn, Phys. Rev. Lett. **111**, 230601 (2013).
[15] H. van Beijeren, Phys. Rev. Lett. **108**, 180601 (2012).
[16] H. Spohn, *The Kardar-Parisi-Zhang equation - a statistical physics perspective, Proceedings of the Les Houches Summer School of Theoretical Physics, 2015* (Oxford University Press, Oxford, 2016).
[17] H. Spohn, Springer Lecture Notes in Physics **921**, 107 (2016).
[18] H. Ohshima, *Theory of Colloid and Interfacial Electric Phenomena* (Academic Press, Amsterdam, 2006).
[19] H. Ohshima, Sci. Technol. Adv. Mater. **10**, 063001 (2009).
[20] H. Ohshima, Langmuir **31**, 13633 (2015).
[21] L. Lizana and A. Y. Grosberg, Euro. Phys. Lett. **104**, 68004 (2013).
[22] M. von Smoluchowski, *Handbuch der Elektrizitat und des Magnetismus, Stationare Strome*, edited by E. Greatz (Barth, Leipzig, 1921).
[23] D. C. Henry, Proc. R. Soc. London, Ser. A **133**, 106 (1931).
[24] J. Ennis and L. R. White, J. Colloid Interface Sci. **185**, 157 (1997).
[25] A. L. Barabasi and H. E. Stanley, *Fractal Concepts in Surface Growth* (Cambridge University Press, Cambridge, 1995).
[26] T. Halpin-Healy and Y.-C. Zhang, Phys. Rep. **254**, 215 (1995).
[27] D. Forster, D. R. Nelson, and M. J. Stephen, Phys. Rev. A **16**, 732 (1977).